Fluorescent DNA Nanotags Based on a Self-Assembled DNA Tetrahedron

Hayriye Özhalıcı-Ünal and Bruce A. Armitage*

Department of Chemistry and Center for Nucleic Acids Science and Technology, Carnegie Mellon University, 4400 Fifth Avenue, Pittsburgh, Pennsylvania 15213-3890

ABSTRACT Progress in fluorescence detection and imaging technologies depends on the availability of fluorescent labels with strong light absorption/emission characteristics. We have synthesized intercalator dye arrays on a compact 3-dimensional DNA-tetrahedron nanostructure. The template tolerates the structural distortions introduced by intercalation and allows concentration of multiple fluorophores within a small volume, resulting in brightly fluorescent nanotags with effective extinction coefficients in the order of 10^6 M^{-1} cm^{-1}. Efficient energy transfer from intercalated donor dyes to covalently attached acceptor dyes in the nanotags allows the emission wavelength to be shifted to the red relative to the excitation light, providing wavelength tunability. The compact nature of the supramolecular DNA tetrahedron also provides a protective medium for the fluorophores, leading to improved photostability and enhanced resistance to nuclease digestion, relative to one- or two-dimensional nanotags described previously.

KEYWORDS: DNA nanostructures · fluorescent labels · energy transfer · supramolecular assembly · intercalation

Deciphering complex biological events at the molecular level requires adequate tools to visualize and track interacting biomolecules. Fluorescent labeling of biomolecules is desirable due to the potential for fast signal acquisition, high sensitivity and suitability for multiplex assaying by using fluorophores that emit at different wavelengths.[1] While commonly used small dye molecules offer tunability in spectral and physical characteristics, their relatively low brightness, defined as the product of the molar extinction coefficient (ε) and the fluorescence quantum yield (ϕ_f), complicates the use of such dyes in demanding applications such as single molecule detection.

Arrangement of multiple dye molecules into arrays, on the other hand, can dramatically improve the efficiency of light absorption and also provide efficient energy transfer pathways, allowing fine-tuning of the emission wavelength. The challenge in developing such multichromophore arrays is positioning the fluorophores at predefined spatial positions that prevent self-quenching but promote energy transfer. Nature has already solved this problem in the form of the phycobiliproteins found in photosynthetic cyanobacteria. The protein matrix of these structures encapsulates multiple bilin chromophores with sufficient spatial separation to prevent self-quenching, allowing efficient light harvesting and energy transfer to the reaction center protein.[2] However, once decoupled from the reaction center, phycobiliproteins become intensely fluorescent with brightness values that are 10−100-fold greater than other fluorescent proteins (*e.g.*, GFP) and commonly used fluorescent dyes such as fluorescein or Cy3.

Synthetic mimics of the phycobiliproteins have focused on dendrimers[3] or rigid π-conjugated spacers[4,5] as templates for covalent attachment of fluorophores at defined distances. While these systems efficiently harvest light and permit vectorial energy transfer, they have not found applications as fluorescent labels, possibly because of their large molecular weights and complex syntheses. Oligonucleotides have also been used as scaffolds for multiple covalent attachment of fluorescent dyes, where the phosphate backbone acts as a tunable spacer for the fluorophores, leading to energy transfer tags with multicolor labeling potential.[6−8] As in the nonbiological scaffolds, considerable synthetic expertise is required for assembly of these covalent DNA-based assemblies.

Recently, we reported a novel noncovalent approach to create DNA-templated multichromophore arrays with much higher extinction coefficients and efficient energy transfer capabilities relative to systems involving covalently attached dyes.[9] The DNA template consisted of a branched

*Address correspondence to army@andrew.cmu.edu.

Received for review November 1, 2008 and accepted December 31, 2008.

Published online January 14, 2009.
10.1021/nn800727x CCC: $40.75

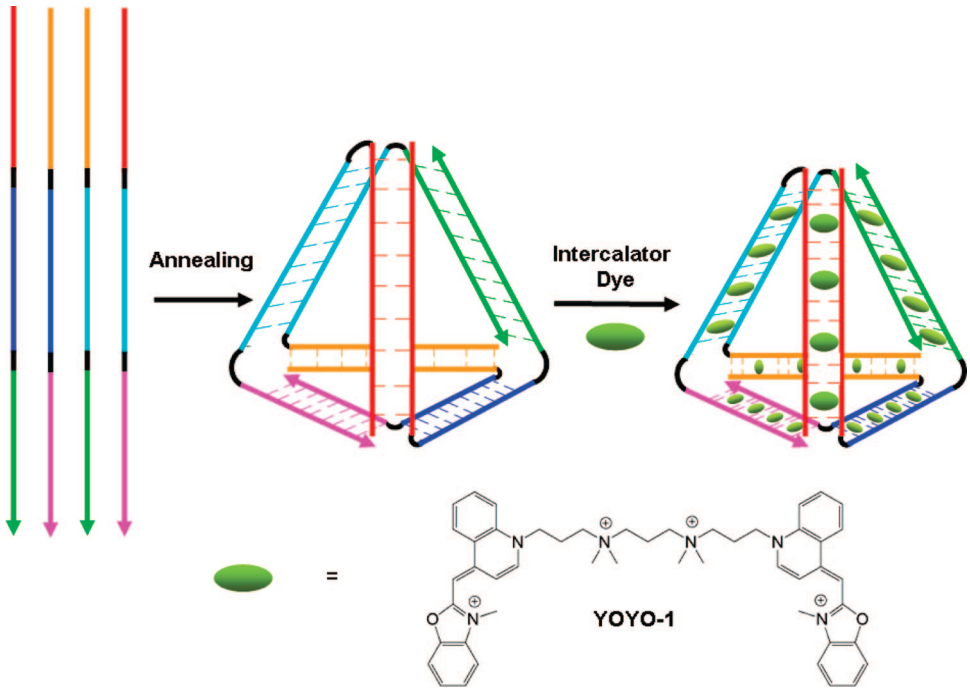

Figure 1. Assembly of DNA-tetrahedron (TH) nanotags. Four strands with partially complementary sequences form the DNA-tetrahedron nanostructure template for the self-assembly of intercalator dyes. Black sections represent two-nucleotide long, single-stranded hinges. DNA strand sequences are given in the Methods section.

2-dimensional nanostructure assembled by hybridizing three or more partially complementary strands *via* Watson–Crick base pairing.[10] These DNA nanostructures served as templates for the assembly of multiple intercalating dyes in a way which concentrated the fluorophores in a small, well-defined region. The inherent steric constraints imposed by the DNA double helix restrict the placement of intercalating dyes to distances and orientations that prevent self-quenching, yet the compact structure of the nanotag allows efficient energy transfer to remote acceptor groups, resulting in bright multichromophore assemblies we termed "DNA nanotags". In the current study we extended this approach to a more compact 3-dimensional assembly based on a tetrahedron (TH) nanostructure.[11,12] The TH nanotag resulting from loading with fluorescent intercalating dyes exhibited several improvements over lower-dimensional analogues, including higher density of fluorophores without significantly compromised brightness, improved photostability, and good resistance to degradation by nuclease enzymes.

RESULTS AND DISCUSSION

Nanotag Design. TH nanotags were assembled by the incubation of intercalating dyes with tetrahedron nanostructures, which were prepared *via* a high-yield, single-step synthesis originally reported by Turberfield and coworkers.[11,12] As shown in Figure 1, four oligonucleotide strands with partially complementary sequences can self-assemble into a tetrahedron consisting of 102 Watson–Crick base pairs. The six edges are 17 base pairs in length and are connected by "hinges" consisting of two unpaired nucleotides that ensure sufficient flexibility to form the tetrahedron. The double-stranded edges of the tetrahedron provide the binding sites for the light-harvesting pintercalating dyes. YOYO-1, the bisintercalating dimer of oxazole yellow,[13,14] was chosen as the intercalator dye because of its high affinity for double-stranded DNA, its high extinction coefficient of 98900 M^{-1} cm^{-1}, and its fluorogenic properties.[15]

Figure 2 compares linear (1D), branched 3-way junction (2D), and tetrahedron (3D) DNA nanotags and illustrates the compact nature of the TH. The approximate length of each edge of the TH is 8.5 nm, calculated by assuming that 8 intercalating chromophores bind to the 17 bp-long edge.

Nanotag Assembly and Characterization. According to the neighbor exclusion principle,[16] intercalation density should saturate at one intercalator for every two base pairs due to steric constraints imposed by the DNA, which must be stretched and unwound to create an intercalation site. Thus, full saturation of the DNA should occur when half of the binding sites are occupied. In theory, the 102 base pairs in the TH should accommodate up to 51 intercalator dyes, or 25 YOYO-1 molecules. However, given the odd number of base pairs

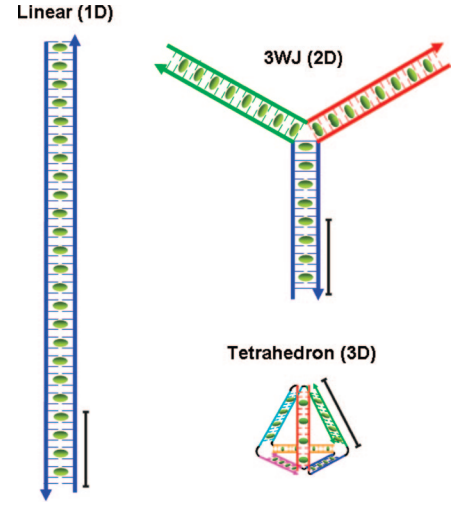

Figure 2. Fluorescent nanotags based on linear (1D), 3-way-junction (2D), and tetrahedron (3D) DNA nanostructures and intercalating dyes (drawn to scale). Scale bar corresponds to ca. 8.5 nm in actual constructs.

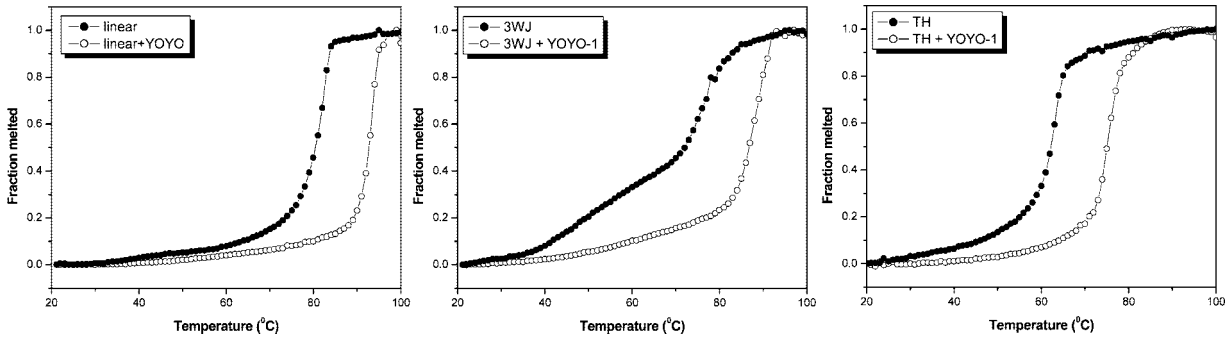

Figure 3. UV-melting curves recorded for tetrahedron (TH) DNA in the absence and presence of YOYO-1. [DNA] = 50 nM nanostructure, [YOYO-1] = 1.3 μM (*i.e.*, approx 1 bis-intercalator dye per 4 base pairs).

in each edge and the symmetry of the tetrahedron nanostructure, it is likely that only 4 bisintercalators bind per edge, giving 48 total intercalated chromophores.

The DNA nanostructures were assembled by a simple thermal annealing process. Figure 3 illustrates UV melting curves recorded for the three structures with and without saturating amounts of the bisintercalating dye YOYO-1. While the branched 3WJ structure exhibits a broad low temperature transition in the absence of YOYO-1, all three nanostructures undergo cooperative melting transitions in the presence of the dye. Moreover, intercalation of YOYO-1 increases the thermal stability of the DNA structures by approximately the same amount, regardless of the dimensionality of the nanostructure. These results indicate that the DNA-dye nanostructures are fully assembled at room temperature.

The impact of the intercalating dye on the TH nanostructure was also examined by nondenaturing gel electrophoresis. The TH migrates as a single band through the gel, even when the intercalator dye is added before electrophoresis (Figure 4). This indicates that the 3D nanostructure is preserved in the presence of the dye. Interestingly, the mobility of the TH is unchanged by intercalation of YOYO-1, whereas the linear and 3WJ DNA mobilities are retarded by the dye.

Optical Spectroscopy. Figure 5 illustrates the UV−vis absorbance spectra recorded for YOYO-1 in the presence of the linear, branched, and TH nanostructures. The unbound dye has maximum absorbance at 450 nm with a weaker band at 488 nm, but the situation is reversed in the presence of DNA. This is because the unbound dye adopts a collapsed conformation in which the two chromophores are stacked into an "H"-dimer structure. Intercalation into DNA separates the chromophores and restores the monomer spectrum. The hypochromic effect is also characteristic of intercalated dye and the similarity among the three spectra indicates comparable amounts of bound dye, regardless of the dimensionality of the DNA template. While the binding constant of YOYO-1 for linear DNA has not been reported, we expect $K_b \geq 10^9\ M^{-1}$, based on the binding constant for the monointercalating YO-PRO-1[17] and prior work on a bisintercalating ethidium dye.[18] Thus, virtually all of the dye should be bound under these conditions. The nanostructure concentration was 50 nM and the absorbance was 0.09, giving an extinction coefficient of $\varepsilon = 1.8 \times 10^6\ M^{-1}\ cm^{-1}$ at 488 nm. This is comparable to phycobiliproteins and approximately 30-fold greater than enhanced GFP.[19]

Although the absorption spectra of the intercalator dye in the presence of the three nanostructures are similar, significant differences are observed in the respective fluorescence intensities (Figure 6). As the dye is titrated into a solution of the DNA nanostructure, the fluorescence is consistently weaker for the TH and levels off at a lower concentration. Intermediate behavior is observed for the 2D branched nanostructure. (Similar results were obtained in flow cytometry experiments described in Supporting Information.) All three DNA templates have similar sequence composition (47−48% GC) so the difference in fluorescence intensity is unlikely to be due to the known sequence dependence of fluorescence quantum yield for this dye.[20] An alternative possibility is that one or more of the chromophores insert into the junction regions linking different helices in the 2- and 3-D structures. Since these dyes will not be as constrained as a fully intercalated dye, the quantum yield would be expected to be lower. In addition, such dyes could serve as traps for energy migrating through the assembly, further reducing the

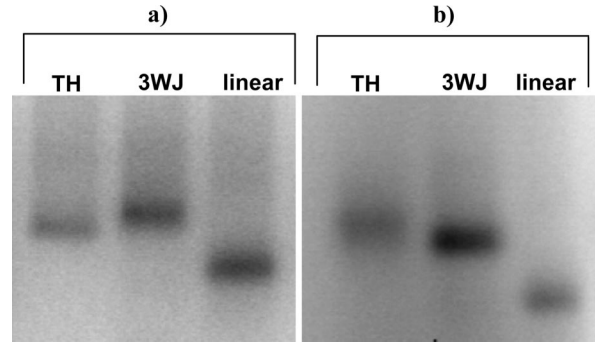

Figure 4. Visualization of YOYO-1 intercalation on agarose gel. Shown are TH, 3WJ, and linear nanostructures (a) loaded with YOYO-1 and incubated for 1 h prior to electrophoresis, and (b) electrophoresed in the absence of YOYO-1 and then stained with ethidium bromide.

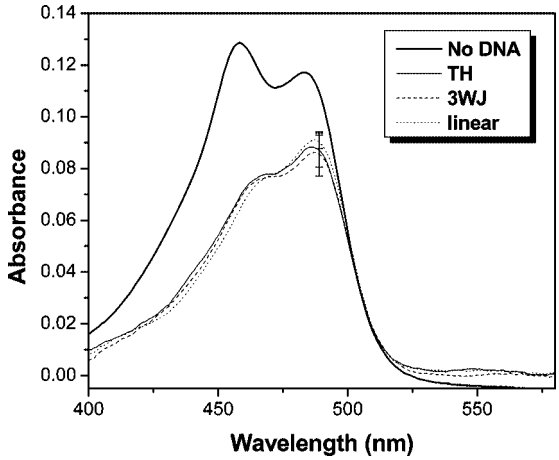

Figure 5. Comparison of absorbance spectra of YOYO-1 in the presence of TH, 3WJ, and linear nanostructures, and free YOYO-1. A 50 nM portion of DNA nanostructure was mixed with 1.28 μM YOYO-1 (*i.e.*, one bisintercalator dye per 4 DNA bps); spectra were acquired after 1 h incubation at room temperature. Error bars reflect the standard deviation of three independent measurements.

overall intensity. Regardless of the origin, the diminution in fluorescence is not that large. Taking the quantum yield for fluorescence in linear DNA to be approximately 0.5,[20] the corresponding value for the TH is still 0.3, giving a brightness ($\varepsilon \times \phi_f$) of 5.4×10^5 M^{-1} cm^{-1}. This is 16 times greater than enhanced GFP and within a factor of 3 of R-phycoerythrin.

Energy Transfer Experiments. In flow cytometry and fluorescence microscopy, it is useful to have labels that fluoresce in different colors but that can be excited at the same wavelength, such that different populations can be distinguished while using the same light source. Systems in which energy can be transferred from donor to acceptor molecules through energy transfer (ET) are suitable candidates for such multicolor labeling.[21] One of the most appealing features of the 2-D nanotags we reported previously was the highly efficient ET from intercalated YOYO-1 to terminal acceptor dyes such as

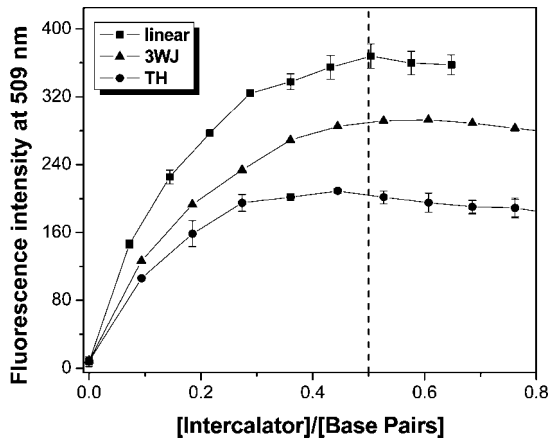

Figure 6. Change in the fluorescence intensity of YOYO-1 bound to TH, 3WJ, and linear DNA nanostructures by increasing ratio of intercalator dyes per base pair. Samples containing 5.1 μM base pairs DNA (50 nM nanostructure) were titrated with 0.2 μM aliquots of YOYO-1.

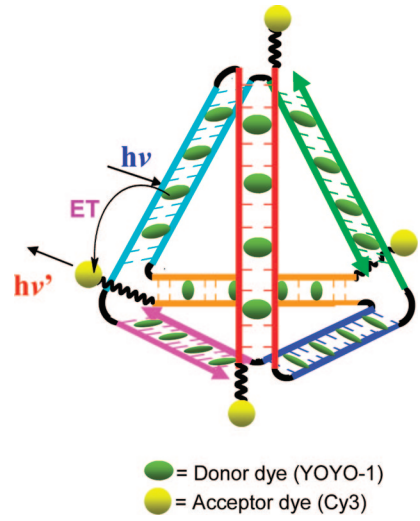

Figure 7. Schematic description of ET in a tetrahedron nanotag loaded with YOYO-1 intercalated dyes and covalently attached Cy3 acceptor dyes.

Cy3 or WellRed-D2. We performed similar experiments with the TH nanotags by attaching 1−4 Cy3 acceptor dyes to the 5′-termini of the DNA strands, which positions them at the helix junction points on the tetrahedron (Figure 7). Fluorescence spectra demonstrate that the ET efficiency increases monotonically with the number of Cy3 acceptors, reaching a maximum of 95% (Figure 8). However, even a single Cy3 is able to quench 52% of the donor emission.

Such a high ET efficiency is likely due to the compact nature of the TH, which localizes all intercalated dye molecules within a diameter of less than 10 nm, similar to the critical transfer distance of 7.3 nm for the YOYO-1/Cy3 pair assuming ET occurs *via* the Förster dipole coupling mechanism. (YOYO-1 that is bound very close to a Cy3 acceptor might also undergo ET *via* an exchange mechanism.) In addition, energy migration among the cointercalated chromophores is also possible,[22] particularly within a given edge of the TH, al-

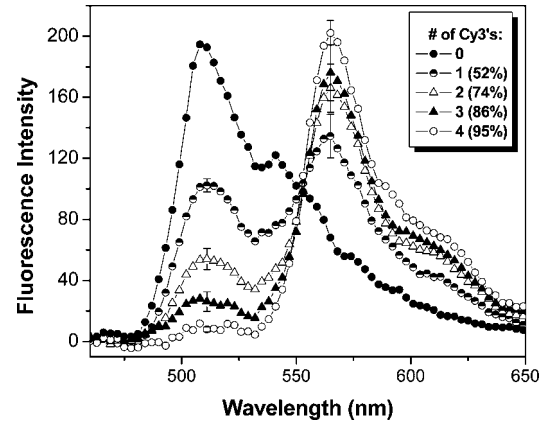

Figure 8. Fluorescence emission of TH nanotags with 0−4 covalently attached Cy3 molecules. Spectra acquired by excitation at 440 nm. Samples contained 50 nM DNA tetrahedron and 1.28 μM YOYO-1. ET efficiencies given in legend were determined by the % decrease in the YOYO-1 emission at 509 nm.

though the twist of the DNA helix might minimize this process for adjacent dyes. Thus, the TH acts as an antenna to harvest light with very strong efficiency and transfers the excitation to a lower energy acceptor dye at a nearby helix junction. This indicates that TH nanotags with and without the Cy3 acceptor dyes can be used to label two different species of interest, while being excitable at the same wavelength, as we previously demonstrated for a 3WJ nanotag.[9]

To demonstrate a potential application of these fluorescent TH nanotags, streptavidin-functionalized polystyrene beads were coated with TH nanotags using a biotin molecule covalently attached to the 5′-terminus of one of the DNA strands. As shown in Figure 9, YOYO-1 saturated DNA-TH can act as a bright label. Beads were nonfluorescent when they were unmodified or when they were coated with biotinylated TH nanostructures without the intercalator dyes (curves A and B). Adding YOYO-1 to the beads in the absence of DNA led to significant fluorescence, presumably due to nonspecific interactions between the dye and either the streptavidin protein or the polystyrene bead (curve C). Interestingly, addition of nonbiotinylated DNA and YOYO-1 gave the same result as YOYO-1 alone, indicating better binding of the dye to the beads than to the low concentration of free DNA (curve D). However, the beads became 10-fold brighter when they were coated with the biotinylated, YOYO-1 loaded TH-nanotags. The amount of dye and DNA present in experiments D and E are the same, yet the fluorescence is 10-fold higher in the latter. This suggests that immobilizing the DNA on the bead leads to higher effective concentrations, which competes more effectively with the bead for the dye than when the TH is diluted at nanomolar concentrations into the surrounding solution. Meanwhile, the increase in brightness is indicative of a higher quantum yield for DNA-intercalated *versus* polymer-adsorbed dye and shows that these noncovalent assemblies are sufficiently stable to allow labeling of polymer beads commonly used in flow cytometry-based diagnostics assays.

Photostability Studies. One critical parameter for effective use of fluorescent labels in imaging applications is the photostability of the fluorophores. Stable fluorescence intensity is desired for applications requiring long irradiations such as single molecule spectroscopy or fluorescence imaging of low abundance species. Cyanine dyes are known to undergo photobleaching *via* reaction with singlet oxygen, which is produced by a small fraction of the dye excited-state that intersystem crosses to the triplet manifold.[23−25] The TH nanotags were expected to minimize this reaction path by virtue of intercalation of the dyes into the DNA matrix, which should not only restrict access of molecular oxygen to the dye excited state, but also hinder reaction with any singlet oxygen that does get produced. Prior work by Kanony and co-workers showed that DNA-intercalated

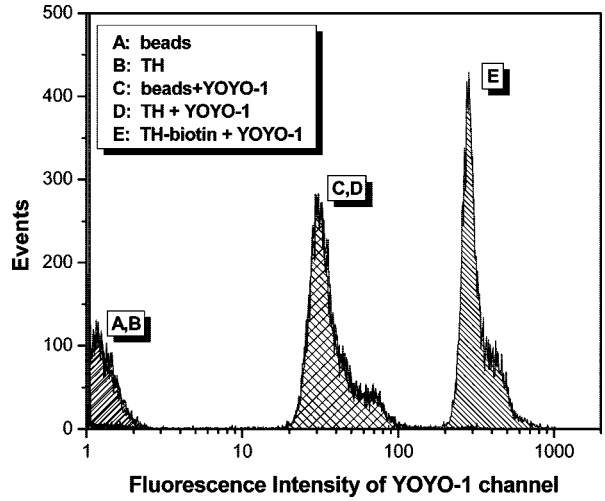

Figure 9. Flow cytometry analysis of TH-labeled streptavidin-coated polystyrene beads. Empty beads (A) and beads coated with biotinylated TH without YOYO-1 (B) exhibited background fluorescence/light scattering only. Nonspecific interaction of YOYO-1 with the beads led to modest fluorescence, even in the presence of free DNA TH (C and D). When beads were coated with biotinylated TH nanotags intercalated with YOYO-1 (E), 10-fold greater intensity was obtained.

oxazole yellow dyes were less prone to reaction with singlet oxygen and were found to exhibit slower decay of fluorescence intensity under prolonged irradiation, in comparison to fluorophores which were free in solution.[26]

We compared the photostabilities of YOYO-1 intercalated in linear (1D) and TH (3D) nanostructures. As shown in Figure 10, the TH-intercalated dye underwent less than 5% decrease in fluorescence intensity after 50 min of irradiation with a Hg arc lamp. In contrast, nearly 30% of the fluorescence was lost from dye that was intercalated into the linear DNA template. Interestingly, the dye absorption spectrum was not perturbed by the irradiation, even in the linear DNA experiment where a substantial decrease in fluorescence intensity was observed (data not shown). This indicates that the loss of fluorescence shown in Figure 10 is due to dam-

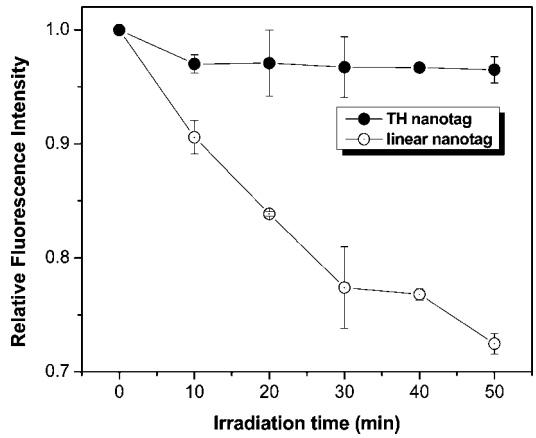

Figure 10. Comparison of photostability of YOYO-1 intercalated to TH and linear DNA templates. Fluorescence intensity at emission maximum of YOYO-1 (509 nm) was recorded initially and after every 10 min irradiation with visible light.

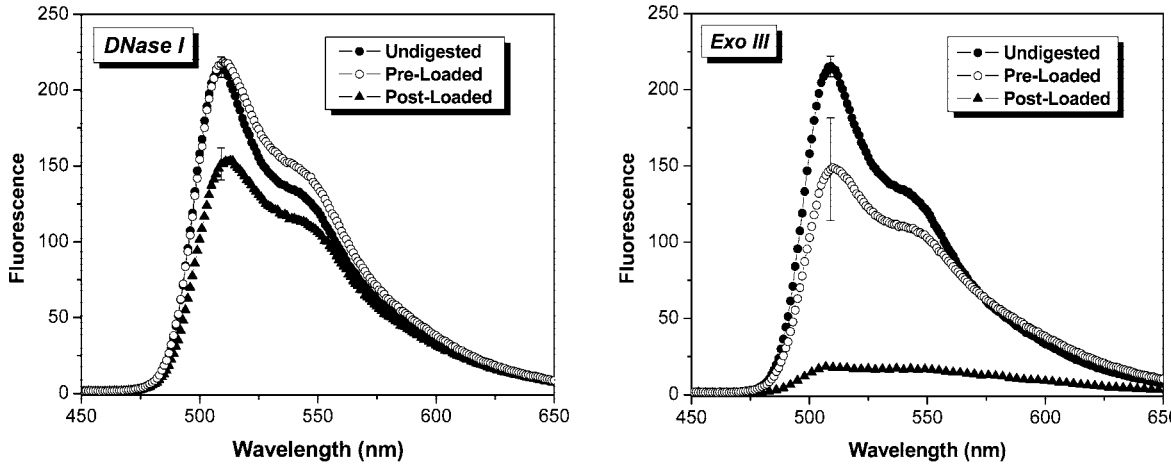

Figure 11. Fluorescence spectra of TH-nanostructures digested with nuclease enzyme either in the absence ("preloaded") or presence ("postloaded") of YOYO-1, in comparison to nanotags which were not treated with nucleases. The greater fluorescence retained by TH-nanostructures digested in the presence of the dye indicates that intercalation protects the DNA from enzymatic degradation.

age to the DNA template rather than to the dye. Kanony and co-workers made similar observations and attributed it to photoinduced oxidation of the DNA, specifically at guanine residues.[26] The oxidized guanines can then serve as electron transfer quenchers of the dye, resulting in decreased fluorescence intensity without photobleaching of the dye. The ability of the TH nanostructure to resist photodamage is a significant advantage relative to a linear DNA template and will be the subject of further study.

Biochemical Stability. To more precisely define the range of conditions in which DNA nanotags can be used as fluorescent labels, we investigated the biochemical stability of these noncovalent assemblies. While the TH nanotags exhibit excellent photostability, it is also possible that the DNA backbone could be degraded by nuclease enzymes that are present in biological samples. This would release the dyes into solution and diminish the fluorescence brightness of whatever was labeled by the nanotag.

Previous studies have shown that bisintercalating dyes improve the stability of a DNA duplex against endonuclease degradation, presumably because of the lengthening and unwinding of the duplex that occurs in response to intercalation.[27] Hence, TH nanotags were also expected to be less prone to hydrolysis by nuclease enzymes. This was verified by monitoring the fluorescence intensity of the nanotags treated with endo- (DNase I) or exonuclease (Exo III) before or after loading with intercalator dyes. As shown in Figure 11, TH nanostructures loaded with intercalators *prior* to exposure to the enzyme (*i.e.*, "preloaded" samples) retained significantly higher fluorescence for both nucleases, consistent with a protective effect of the intercalator dye.

The susceptibility of the DNA to enzymatic degradation was also compared for nanotags of different dimensionalities. As shown in Figure 12, the 3D TH nanotag was significantly more resistant than the other two against the endonuclease (DNase I), likely because of the significantly shorter edges of the more compact TH nanostructure. Meanwhile Exo III, which attacks the 3′ end of the DNA strand and removes one nucleotide at a time, also exhibited lower activity against the TH than the 3WJ and comparable activity with the linear nanostructure, despite the fact that there are more 3′-termini in the TH than the 3WJ and linear nanostructures (4 versus 3 and 2, respectively). Note that in practical applications, exonuclease activity can be further inhibited if the strands are designed in a way that allows ligation of adjacent termini[12] or by using terminal modifications such as phosphorothioates. The improved resistance to nuclease degradation for the TH nanostructure could allow for use in analyzing complex biological samples without having to purify or otherwise treat the sample prior to analysis by flow cytometry or spectroscopy.

DISCUSSION

Research in the past decade has redefined the fundamental biomolecule DNA as a unique nanoconstruction

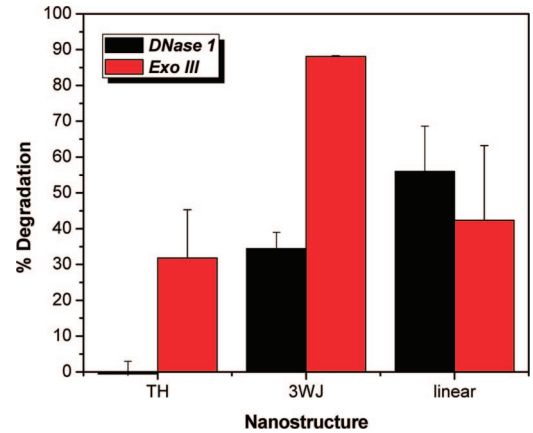

Figure 12. Loss of fluorescence due to digestion with DNase I (black) or Exo III (red) for different DNA nanotags. All samples were preloaded with a saturating amount of the bisintercalator dye YOYO-1 prior to enzymatic digestion.

material.[11,12,28−32] Various rational design approaches have led to DNA nanostructures of different dimensionalities and potential functions. We previously chose to induce fluorescent dye assembly on a two-dimensional 3WJ nanostructure to create bright fluorescent nanotags.[9] With our current research we extended this idea into three dimensions by using a DNA tetrahedron (TH) nanostructure[11,12] as a template for assembly of an intercalating cyanine dye array. In addition to providing a more compact structure, the 3D TH nanotag exhibits substantial improvements in both photo- and biochemical stability.

In assembling the TH nanotag, some concern arose as to whether the constrained DNA nanostructure would be capable of accommodating a large number of intercalating dyes. The intercalation process imposes considerable strain on the DNA structure, which must extend and unwind to create a binding pocket for each dye.[33] In the case of linear and branched templates, each arm of the DNA nanostructure can simply extend further from the core and binding up to the expected saturation point of two base pairs/intercalator is observed. It was not clear how the 3D tetrahedral template would respond to the bisintercalating dye, but as shown in Figures 5 and 6, a substantial amount of dye is bound by the DNA, and gel electrophoresis indicates that the tetrahedron remains intact after addition of the dye (Figure 4). Although fluorescence titrations suggest that the DNA saturates at approximately three base pairs/intercalator (Figure 6), the UV−vis absorption spectra (Figure 5) indicate that the amount of bound dye is similar for the linear, branched, and tetrahedral templates. Therefore, the difference in fluorescence intensity observed in Figure 6 appears to be due to a lower average quantum yield for the dye bound to the TH compared with the linear and 3WJ templates, which could reflect binding of some oxazole yellow groups in the hinge regions at the TH vertices.

The minor (ca. 1.8-fold) loss of brightness on assembling the dyes on a 3D template compared with the 1D and 2D analogues is compensated not only by the more compact structure of the tetrahedron but also by improvements in both photo- and biochemical stability. For example, the TH nanotag retains >95% of its initial fluorescence intensity during prolonged irradiation, whereas the analogous linear nanotag loses nearly 30% of its intensity under identical conditions. Whether the enhanced photostability of the TH nanotag is due to (i) less efficient singlet oxygen production, (ii) lower inherent reactivity toward singlet oxygen, or (iii) some other factor remains to be determined.

The 3D tetrahedral nanotag also exhibits impressive resistance to nuclease degradation; thus, the fluorophore binding sites on the DNA template stay intact and lead to high brightness even after extended incubation with endo- or exonuclease enzymes. These results indicate that the TH nanotags can be used in complex biological samples, provided that dissociation of the noncovalently bound dye from the DNA template does not cause problems, as we observed previously for 2D nanotags based on a 3WJ DNA template.[9] Efficient strategies for covalent attachment of dyes to DNA have been reported[34] and will lead to even more stable nanotags that might find use for intracellular imaging and detection experiments.

On the basis of the evidence provided here with the tetrahedral DNA scaffold, this novel approach can be extended to other more compact DNA nanostructures. Rational design of DNA nanoarchitectures can result in templates of even higher densities of fluorophore binding sites in relatively small volumes of space, as in the examples of a 3D octahedron[32] and 2D nanostructures consisting of 8- and 12-armed junctions[35] recently reported in the literature. The results obtained in this study demonstrate that a compact 3D nanostructure provides a protective environment for the fluorophores, which leads to intense and stable optical signals. As the ratio of binding sites per unit volume of the nanostructure increases, brighter and smaller nanotags can result and find various applications.

Because of the availability of well-established methods to functionalize DNA for conjugation to antibodies, proteins, peptides, or other nucleic acids, these nanotags can be utilized to label and track biomolecules. In that sense they can find similar applications as the fluorescent polymer[36] and silica[37] nanoparticles that have been developed for multiplex bioassays. In addition to ease of synthesis and conjugation to biomolecules, having the ability to control both the number and the proximity of fluorophores on a 3D DNA template as opposed to being embedded irregularly in a matrix will be advantageous. The DNA template also allows rational manipulation of the energy transfer efficiency by varying the number and location of acceptor fluorophores. Thus, nanotags constructed from an intercalating donor and terminal acceptor can yield more than two "colors" by tuning the ET efficiency over the range from 0−100% and relying on ratiometric measurements.

METHODS

Materials. DNA oligonucleotides were purchased from Integrated DNA Technologies, Inc. (www.idtdna.com) as lyophilized powders. Sequences of the DNA oligonucleotides used to generate tetrahedron, 3WJ, and linear nanostructures are shown below.

The following sequences were used for the tetrahedron nanostructure:

TH-S1: 5′-ACATTCCTAAGTCTGAAACATTACAGCTTGCTACACGAGAAGAGCCGCCATAGTA-3′.

TH-S2: 5′-TATCACCAGGCAGTTGACAGTGTAGCAAGCTGTAATAGATGCGAGGGTCCAATAC-3.′

TH-S3: 5′-TCAACTGCCTGGTGATAAAACGACACTACGTGGGAATCTACTATGGCGGCTCTTC-3′.

TH-S4: 5′-TTCAGACTTAGGAATGTGCTTCCCACGTAGTGTCGTTTGTATTGGACCCTCGCAT-3′.

The same sequences with biotin conjugated to 5′-end of TH-S2, and Cy3 conjugated to the 5′-end of TH-S1, TH-S2, TH-S3, and TH-S4 were also purchased and used for energy transfer and bead-labeling experiments.

The following sequences were used for the 3WJ nanostructure:

3WJ-S1: 5′-ACGGACATCTAGGTATCCTGAGCAGGTGGCGAGAGCGACGATCCATACAATCAATTGGT GAATGTTAG-3′.

3WJ-S2: 5′-CTAACATTCACCAATTGATTGTATGGATCGTCGCAGAGTTGACCGGAAATACGCGCTCAT AACTTGGT-3′.

3WJ-S3: 5′-ACCAAGTTATGAGCGCGTATTTCCGGTCAACTCTTCTCGCCACCTGCTCAGGATACCTAG ATGTCCGT-3′.

The following sequences were used for the assembly of linear nanostructure:

Linear S1: 5′-ACATTCCTAAGTCTGAAGAAGAGCCGCCATAGTATATCACCAGGCAGTTGAGTGTAG CAAGCTGTAATATGCGAGGGTCCAATACACGACACTACGTGGGAA-3′.

Linear S2: 5′-TTCCCACGTAGTGTCGTGTATTGGACCCTCGCATATTACAGCTTGCTACACTCAACTGCC TGGTGATATACTATGGCGGCTCTTCTTCAGACTTAGGAATGT-3′.

The DNA-intercalating dye YOYO-1 was purchased from Molecular Probes (now Invitrogen). Streptavidin-coated polystyrene beads (6.9 μm diameter) were purchased from Spherotech, Inc. DNase I, and Exo III were purchased from New England Biolabs. Calf thymus DNA was purchased from Sigma-Aldrich.

Assembly of Fluorescent DNA Tetrahedra (TH) Nanostructures. Solutions of oligonucleotide strands were prepared in 10 mM aqueous sodium phosphate buffer (pH = 7.0) and stored at −4 °C. Varian Cary 3 Bio UV−vis spectrophotometer was used to determine concentrations. A DNA-solution containing 1.0 μM of each strand in TM buffer (10 mM Tris, 5 mM $MgCl_2$) was prepared, heated to 95 °C for 2 min, and cooled in ice bath. YOYO-1 concentrations were determined in DNA using a spectrophotometer with $\varepsilon = 98900\ M^{-1}\ cm^{-1}$. Assembled DNA TH nanostructures were incubated with saturating amounts of YOYO-1 (1 dye: 4 base pairs) for 30 min at room temperature. Fluorescent DNA-nanostructures were visualized on 1% agarose gel. Melting temperatures were determined by monitoring the absorbance of 50 nM DNA with and without 1.28 μM YOYO-1 at 260 nm while increasing temperature at a rate of 1 °C/min and then calculating the first derivative of the resulting melting curve.

Fluorescence Measurements. All fluorescence studies were conducted on a Photon Technologies International fluorimeter. Titration experiments: 50 nM solutions of DNA TH nanostructures were titrated with 0.24 μM aliquots of YOYO-1. The spectral bandwidth for both excitation and emission monochromators were chosen to be 5 nm. ET experiments: 50 nM solutions of YOYO-1 saturated, Cy3-labeled DNA TH nanostructures were prepared, where one or more strands had a 5′-conjugated Cy3. Samples were excited at 430 nm, and fluorescence was measured from 450−650 nm. ET efficiency (E) was calculated according to the formula: $E = (1 - F_{DA})/F_D$ where F_{DA} and F_D are the intensities of the donor (YOYO-1) at 509 nm in the presence and absence of acceptor (Cy3), respectively.

Photostability Experiments. Solutions of 50 nM DNA-TH and calf thymus DNA having the same base pair concentration (5.1 μM) saturated with YOYO-1 (4 base pairs per dye) were prepared. Samples in fluorescence cells were irradiated by a 150 W Hg(Xe) lamp. A bandpass filter (Oriel, filter no. 59830, 325 nm $< \lambda <$ 525 nm) and a neutral density filter that blocked 90% of the incident light were placed between the lamp and the sample for selective irradiation. Both absorbance and fluorescence spectra (excitation at 440 nm, emission at 509 nm) were acquired before and after every 10 min irradiation and cells were wrapped in aluminum foil between scans and irradiation to prevent unintentional photobleaching of the dyes.

Nuclease Digestion Experiments. 50 nM DNA (linear, 3WJ or TH) solutions saturated with YOYO-1 were incubated with 6 μL of the nuclease in 150 μL of final volume of the buffer supplied by the vendor for 1 h at 37 °C. To determine the effect of the intercalator dye on the nuclease stability, nanostructures were also treated in the absence of YOYO-1. The digested DNA samples were then poststained with the same concentration of YOYO-1. The nuclease activities were calculated as the percent decrease of the fluorescence intensity at 509 nm after being treated with the nuclease.

Microbead Labeling with Fluorescent DNA Nanostructures. DNA nanostructures prepared from biotin containing strands were saturated with YOYO-1. Streptavidin-coated polystyrene beads were suspended in 50 μL of calcium- and magnesium-free PBS so that there were 10^6 beads in the solution. The beads were then incubated with solutions containing 9.3 pmoles of DNA nanotag (saturated with YOYO-1) for 30 min and washed two times with 150 μL of PBS. Samples were resuspended in 0.6 mL PBS. Labeled beads were analyzed by fluorescence activated cell sorting (FACS) using a Coulter Epix Elite flow cytometer (Beckman-Coulter, Fullerton, CA) equipped with a 488 nm argon-ion laser. The following dichroic lenses (DL)/band-pass (BP) filters were used: 550DL/525BP (PMT2), and 600DL/575 BP (PMT3). YOYO-1 was detected in PMT2 channel, and Cy3 was detected in PMT3 channel.

Acknowledgment. We are grateful to Yehuda Creeger for expert technical assistance with flow cytometry experiments and to Dr. Andrea Benvin and Prof. Marcel Bruchez for helpful discussions. This work was supported by Grant No. 44470-AC4 of the American Chemical Society's Petroleum Research Fund, made possible through the generosity of the original donors who created the 1944 Fund.

Supporting Information Available: Flow cytometry results demonstrating energy transfer on TH-nanotag-labeled microspheres and comparing 1D (linear), 2D (3WJ), and 3D (TH) nanotags. This material is available free of charge *via* the Internet at http://pubs.acs.org.

REFERENCES AND NOTES

1. Waggoner, A. Fluorescent Labels for Proteomics and Genomics. *Curr. Opin. Chem. Biol.* **2006**, *10*, 62–66.
2. Glazer, A. N. Light Guides. Directional Energy Transfer in Photosynthetic Antenna. *J. Biol. Chem.* **1989**, *264*, 1–4.
3. Balzani, V.; Ceroni, P.; Maestri, M.; Saudan, C.; Vicinelli, V. Light Harvesting Dendrimers. *Curr. Opin. Chem. Biol.* **2003**, *7*, 657–665.
4. Rybtchinski, B.; Sinks, L. E.; Wasielewski, M. R. Combining Light-Harvesting and Charge Separation in a Self-Assembled Artificial Photosynthetic System Based on Perylenediimide Chromophores. *J. Am. Chem. Soc.* **2004**, *126*, 12268–12269.
5. Hindin, E.; Forties, R. A.; Loewe, R. S.; Ambroise, A.; Kirmaier, C.; Bocian, D. F.; Lindsey, J. S.; Holten, D.; Knox, R. S. Excited-State Energy Flow in Covalently Linked Multiporphyrin Arrays: The Essential Contribution of Energy Transfer between Nonadjacent Chromophores. *J. Phys. Chem. B* **2004**, *108*, 12821–12832.
6. Li, Y.; Cu, Y. T. H.; Luo, D. Multiplexed Detection of Pathogen DNA with DNA-Based Fluorescence Nanobarcodes. *Nat. Biotechnol.* **2005**, *23*, 885–889.
7. Vyawahare, S.; Eyal, S.; Mathews, K. D.; Quake, S. R. Nanometer-scale Fluorescence Resonance Optical Waveguides. *Nano Lett.* **2004**, *4*, 1035–1039.
8. Tong, K.; Li, Z.; Jones, G. S.; Russo, J. J.; Ju, J. Combinatorial Fluorescence Energy Transfer Tags for Multiplex Biological Assays. *Nat. Biotechnol.* **2001**, *19*, 756–759.
9. Benvin, A. L.; Creeger, Y.; Fisher, G. W.; Ballou, B.; Waggoner, A. S.; Armitage, B. A. Fluorescent DNA Nanotags: Supramolecular Fluorescent Labels Based on Intercalating Dye Arrays Assembled on Nanostructured DNA Templates. *J. Am. Chem. Soc.* **2007**, *129*, 2025–2034.
10. The concept of a one-dimensional (i.e., linear) DNA nanotag was originally proposed by Glazer and coworkers U.S. Patent 5,763,162 and recently demonstrated by Zhang and Gui: Zhang, Q.; Guo, L.-H. Multiple Labeling of Antibodies with Dye/DNA Conjugate for Sensitivity Improvement in Fluorescence Immunoassay. *Bioconj. Chem.* **2007**, *18*, 1668–1672.

11. Goodman, R. P.; Berry, R. M.; Turberfield, A. J. The Single-Step Synthesis of a DNA Tetrahedron. *Chem. Commun.* **2004**, 1372–1373.
12. Goodman, R. P.; Schaap, I. A. T.; Tardin, C. F.; Erben, C. M.; Berry, R. M.; Schmidt, C. F.; Turberfield, A. J. Rapid Chiral Assembly of Rigid DNA Building Blocks for Molecular Nanofabrication. *Science* **2005**, *310*, 1661–1665.
13. Larsson, A.; Carlsson, C.; Jonsson, M.; Albinsson, B. Characterization of the Binding of the Fluorescent Dyes YO and YOYO to DNA by Polarized Light Spectroscopy. *J. Am. Chem. Soc.* **1994**, *116*, 8459–8465.
14. Johansen, F.; Jacobsen, J. P. ^{1}H NMR Studies of the Bis-Intercalation of a Homodimeric Oxazole Yellow Dye in DNA Oligonucleotides. *J. Biomol. Struct. Dyn.* **1998**, *16*, 205–222.
15. Rye, H. S.; Yue, S.; Wemmer, D. E.; Quesada, M. A.; Haugland, R. P.; Mathies, R. A.; Glazer, A. N. Stable Fluorescent Complexes of Double-Stranded DNA with Bis-Intercalating Asymmetric Cyanine Dyes: Properties and Applications. *Nucleic Acids Res.* **1992**, *20*, 2803–2812.
16. Crothers, D. M. Calculation of Binding Isotherms for Heterogeneous Polymers. *Biopolymers* **1968**, *6*, 575–584.
17. Petty, J. T.; Bordelon, J. A.; Robertson, M. E. Thermodynamic Characterization of the Association of Cyanine Dyes with DNA. *J. Phys. Chem. B* **2000**, *104*, 7221–7227.
18. Gaugain, B.; Barbet, J.; Capelle, N.; Roques, B. P.; Lepecq, J. B.; Lebret, M. DNA Bifunctional Intercalators 0.2. Fluorescence Properties and DNA Binding Interaction of an Ethidium Homodimer and an Acridine Ethidium Heterodimer. *Biochemistry* **1978**, *17*, 5078–5088.
19. McRae, S. R.; Brown, C. L.; B., G. R. Rapid Purification of EGFP, EYFP, and ECFP with High Yield and Purity. *Protein Expression Purif.* **2005**, *41*, 121–127.
20. Netzel, T. L.; Nafisi, K.; Zhao, M.; Lenhard, J. R.; Johnson, I. Base-Content Dependence of Emission Enhancements, Quantum Yields, and Lifetimes for Cyanine Dyes Bound to Double-Stranded DNA: Photophysical Properties of Monomeric and Bichromophoric DNA Stains. *J. Phys. Chem.* **1995**, *99*, 17936–17947.
21. Jares-Erijman, E. A.; Jovin, T. M. Imaging Molecular Interactions in Living Cells by FRET Microscopy. *Curr. Opin. Chem. Biol.* **2006**, *10*, 409–416.
22. Fürstenburg, A.; Julliard, M. D.; Deligeorgiev, T. G.; Gadjev, N. I.; Vasilev, A. A.; Vauthey, E. Ultrafast Excited-State Dynamics of DNA Fluorescent Intercalators: New Insight into the Fluorescence Enhancement Mechanism. *J. Am. Chem. Soc.* **2006**, *128*, 7661–7669.
23. Toutchkine, A.; Kraynov, V.; Hahn, K. Solvent-Sensitive Dyes to Report Protein Conformational Changes in Living Cells. *J. Am. Chem. Soc.* **2003**, *125*, 4132–4145.
24. Kanofsky, J. R.; Sima, P. D. Structural and Environmental Requirements for Quenching of Singlet Oxygen by Cyanine Dyes. *Photochem. Photobiol.* **2000**, *71*, 361–368.
25. Renikuntla, B. R.; Rose, H. C.; Eldo, J.; Waggoner, A. S.; Armitage, B. A. Improved Photostability and Fluorescence Properties through Polyfluorination of a Cyanine Dye. *Org. Lett.* **2004**, *6*, 909–912.
26. Kanony, C.; Åkerman, B.; Tuite, E. Photobleaching of Asymmetric Cyanines Used for Fluorescence Imaging of Single DNA Molecules. *J. Am. Chem. Soc.* **2001**, *123*, 7985–7995.
27. Meng, X.; Cai, W.; Schwartz, D. C. Inhibition of Restriction Endonuclease Activity by DNA Binding Fluorochromes. *J. Biomol. Struct. Dyn.* **1996**, *13*, 945–951.
28. Seeman, N. C. DNA Nanotechnology: Novel DNA Constructions. *Annu. Rev. Biophys. Biomol. Struct.* **1998**, *27*, 225–248.
29. Seeman, N. C. At the Crossroads of Chemistry, Biology, and Materials: Structural DNA Nanotechnology. *Chem. Biol.* **2003**, *10*, 1151–1159.
30. Niemeyer, C. M. Nanoparticles, Proteins, and Nucleic Acids: Biotechnology meets Materials Science. *Angew. Chem., Int. Ed.* **2001**, *40*, 4128–4158.
31. Rothemund, P. W. K. Folding DNA to Create Nanoscale Shapes and Patterns. *Nature* **2006**, *440*, 297–302.
32. Shih, W. M.; Quispe, J. D.; Joyce, G. F. A 1.7-Kilobase Single-Stranded DNA that Folds into a Nanoscale Octahedron. *Nature* **2004**, *427*, 618–621.
33. Lerman, L. S. Structural Considerations in the Interaction of Deoxyribonucleic Acid and Acridines. *J. Mol. Biol.* **1961**, *3*, 18–30.
34. Gierlich, J.; Burley, G. A.; Gramlich, P. M. E.; Hammond, D. M.; Carell, T. Click Chemistry as a Reliable Method for the High-Density Postsynthetic Functionalization of Alkyne-Modified DNA. *Org. Lett.* **2006**, *8*, 3639–3642.
35. Wang, X.; Seeman, N. C. Assembly and Characterization of 8-Arm and 12-Arm DNA Branched Junctions. *J. Am. Chem. Soc.* **2007**, *129*, 8169–8176.
36. Bhalgat, M. K.; Haugland, R. P.; Pollack, J. S.; Swan, S.; Haugland, R. P. Green- and Red-Fluorescent Nanospheres for the Detection of Cell Surface Receptors by Flow Cytometry. *J. Immunol. Methods* **1998**, *219*, 57–68.
37. Wang, L.; Tan, W. H. Multicolor FRET Silica Nanoparticles by Single Wavelength Excitation. *Nano Lett.* **2006**, *6*, 84–88.